SEMARAK ILMU PUBLISHING

CFD Letters

Journal homepage:
https://semarakilmu.com.my/journals/index.php/CFD_Letters/index
ISSN: 2180-1363

Characteristics Investigations of Ducted Ka4-70 Series Propeller with Boss Cap Fins Using Numerical and Experimental Method

Berlian Arswendo Adietya[1], I Ketut Aria Pria Utama[1,*], Wasis Dwi Aryawan[1], Dwi Wahyudi[2], Anis Kurniati Arifah[2], Baharuddin Ali[2], Bashofi Cahyo Buwono[2], Miftah[2], Warsito[2]

[1] Department of Naval Architecture, Faculty of Marine Technology, Institut Teknologi Sepuluh Nopember (ITS), Surabaya 60111, Indonesia
[2] Research Center for Hydrodynamics Technology, National Research and Innovation Agency (BRIN), Surabaya 60117, Indonesia

ARTICLE INFO

Article history:
Received 3 June 2023
Received in revised form 5 July 2023
Accepted 7 August 2023
Available online 10 December 2023

Keywords:
CFD; Energy Efficiency; Ka4-70, PBCF; RANSE

ABSTRACT

Unconventional system that are generally adopted for ship propulsion are Ducted Propellers. These devices have recently been studied with medium-fidelity computational fluid dynamics code (based on the potential flow hypothesis) with promising results. Numerical and experimental comparison of ducted propeller with PBCF, case studies with Propeller Ka4-70 used combination ducted and PBCF Divergent. The study was done numerically using computational fluid dynamics (CFD) approach. The solver is based on the Reynolds-Averaged Navier-Stokes (RANS) solutions and turbulence modelling explicit algebraic stress model (EASM). The test data was obtained from CFD simulations consisting of the open propeller and combination Nozzle plus PBCF, but the experiment was done to Nozzle and PBCF only. All measurements were carried out from J = 0 to J = 1.0 with speeds from 0 m/s to 2.445 m/s. The results of the comparative investigation cases between numerical and experiment analysis from Ka4-70 propellers with Nozzle 19A and PBCF Divergent appears that between CFD and experiments, several phenomena are seen. (i) the Ka4-70 propeller without Nozzle 19A and PBCF divergent experienced large pressure at low-speed J = 0.1 to high-speed J = 0.7, but Ka4-70 propeller with Nozzle and PBCF divergent reach highest pressure at J = 0.1 to J = 0.5; (ii) the Ka4-70 propeller without 19A nozzle and PBCF divergent increases the flow velocity at the boss cap fins but does not increase the axial induce velocity, while Ka4-70 propeller using nozzle and PBCF divergent increases the axial induce velocity of the blade, but does not increase the flow velocity of the boss cap fins; (iii) Ka4-70 propeller without Nozzle and PBCF value increase of propeller η_0 to 12% when ESD added in the form of Nozzle and PBCF when J is high, from J = 0.7 to J = 1.0. ; (iv) Ka4-70 propellers with Nozzle 19A and PBCF Divergent has very similar η_0 from J=0 to J=1.0. CFD approach are still appropriate to be relied upon for the overall simulation.

1. Introduction

Ducted Propellers are a commonly employed form of unconventional propulsion systems. They aim to improve propulsion performance by harnessing various physical principles, depending on the

* *Corresponding author.*
E-mail address: kutama@na.its.ac.id (I Ketut Aria Pria Utama)

https://doi.org/10.37934/cfdl.16.2.2441

specific design of the nozzle. These propulsion systems can be categorized as either operating with an accelerating or decelerating duct [1]. The use of an accelerating nozzle has been extensively studied in literature, particularly in scenarios where vessels require high-thrust propulsion at low speeds or when the diameter of the propeller is limited. By incorporating accelerating nozzles, the duct increases the flow rate through the propeller, resulting in more efficient loading, while also generating positive thrust through the nozzle itself.

The origins of this conceptual idea can be traced back to [2, 3], although the works of [4] are considered to be some of the most comprehensive studies on the performance and design principles of ducted propellers. These research studies provide a broad overview of the influence of various geometric parameters of nozzles on their effectiveness. They combine theoretical considerations and precise measurements, establishing connections between non-dimensional parameters and the performance of propellers under both high and low load conditions. Among the examined nozzle profiles, the number 19A stands out as an ideal compromise, demonstrating comparable performance in both towing and pushing scenarios, even when compared to significantly longer nozzles.

However, in any scenario, these configurations might pose difficulties when it comes to retrofitting. On the other hand, the adoption of an Energy Saving Device (ESD) offers a more convenient solution as it requires minimal modifications to the ship's hull, rudder [5], and/or stator fins [6]. This allows for compliance with the Energy Efficiency Operational Index (EEOI) requirements, which is particularly beneficial for existing ships [7]. Among the widely favoured ESD components are Propeller Boss Cap Fins (PBCF). These fins, typically equal in number to the propeller blades, are affixed to the hub boss cap at a minimal angle of attack [8]. The installation process for PBCF is the most economical and straightforward, involving a mere replacement of the hubcap.

The combination of an ESD in the form of a Ducted Propeller can increase propeller thrust, while a PBCF can improve propeller efficiency. These enhancements are beneficial for the performance of commercial ships or traditional fishing vessels, especially during fishing activities, as they indirectly aid the vessel's operations due to the influence of the fishing gear [9] and catamaran type fish vessel [10]. It is also possible to use these technologies on submarines because submarine propellers require specific criteria to provide a larger amount of thrust while operating silently [11] and glass bottom tourism boat [12]. Several studies on ducts, such as the influence of a Pre-Duct in a Ship on Propeller-Hull, have explained that the addition of a pre-duct tends to increase the hull's efficiency while decreasing the propeller's efficiency in open water [13]. Research on the influence of ducts on the performance of Darrieus hydro-turbines has shown that the simulation results indicate an increase in the power coefficient and torque coefficient [14]. Also, the effect of the actuator disk thickness on the results, it was seen that the implementation of small thickness not only requires a finer mesh but also increases the run-time of the simulations [15]. The variation in propeller angle has been studied in terms of twist blade, which explains that the tangential velocity of a propeller with a greater number of blades is the highest [16].

Over the past years, most turbulence models have neglected the effort required to maintain singularity in turbulence modelling [17], leaving a significant gap in research. However, the Explicit Algebraic Stress Model (EASM) has emerged as a promising approach compared to the traditional linear eddy-viscosity model. In the EASM, the Reynolds stress in a two-dimensional turbulence model is obtained by transforming the differential form of the turbulent equations into an explicit algebraic expression. This expression is then improved by incorporating an explicit nonlinear Reynolds stress model, taking advantage of the eddy viscosity assumption. The EASM offers several advantages over the Algebraic Reynolds Stress Model (ARSM), such as better numerical efficiency and addressing the limitations of the linear eddy viscosity model. It accurately captures the anisotropy effect of Reynolds

stress, effectively avoids numerical singularities, enhances model stability, and performs more efficiently in terms of CPU operations compared to the Reynolds Stress Turbulence Model (RSTM) [18].

The significance of this research compared to other studies lies in its objective to concurrently enhance thrust and propulsion efficiency of ships while ensuring affordability. It takes into account future prospects for operational cost savings and reduction in ship investment expenses, considering not only fuel conversion but also maximizing ship propulsion. Therefore, the study combines two ESD, specifically the Propeller Boss Cap Fins (PBCF) and Ducted propeller, with a case study focusing on the Ka4-70 propeller. The analysis predominantly employs CFD methods. In terms of turbulence modelling, the solver utilizes RANSE and an explicit algebraic stress model (EASM).

2. Methodology

Propeller performance parameter is obtained using numerical method by carrying out CFD analysis which calculated by several factor consisting of thrust (K_T) and torque (K_Q) coefficients and efficiency (η_0).

2.1 Modelling

Table 1 shows the main dimension of the scaled propeller which used Kaplan-series with Nozzle 19A and PBCF Divergent.

Table 1
Main dimension of propeller [19]

Type	Unit	Kaplan-Series
Dimension (D)	mm	300
The number of blades	-	4
Expanded area ratio (Ae/Ao)	-	0.7
Pitch of ratio	-	1.2
Angular velocity	Rpm	489
Length of duct (L_D)	mm	0.5D
Clearance between duct and propeller	mm	3

This study uses Kaplan-series as the propeller with Nozzle 19A and PBCF Divergent. The principal dimension of the scaled model, shown in Table 1. The fins selected for the analysis used Sobol design [20] (see Table 2) which indicated value increase for net energy efficiency to 1.3%. Therefore, the design was used as a reference for the application of boss cap fins to increase efficiency on the Ka4-70 propeller.

Figure 1(a) shows the CFD model while Figure 1(b) shows the experimental test model with scaled size applied. The Ka4-70 Propeller is attached with Nozzle 19A and PBCF divergent which is subjected to an open water test with the output value of thrust and torque, subsequently it able to obtain the efficiency value that occurs.

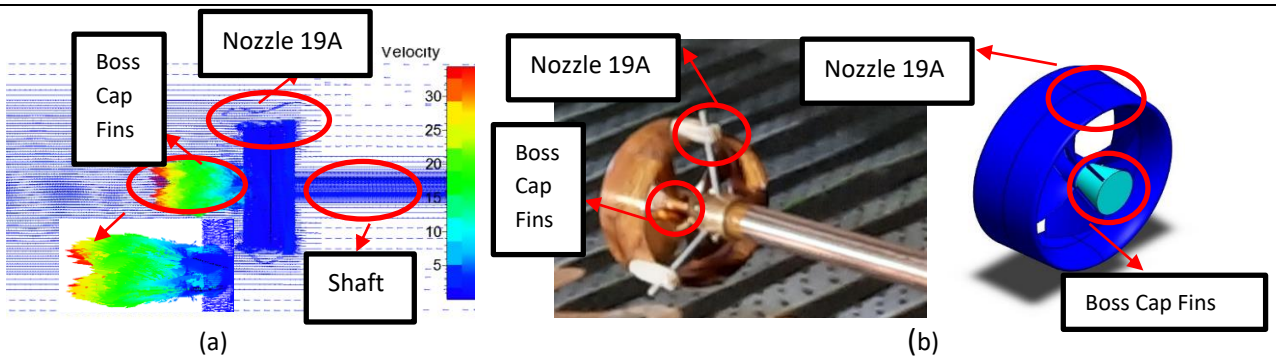

Fig. 1. Propeller Ka4-70 with Nozzle 19A and PBCF divergent (a) CFD model (b Experiment model

Table 2
Sample of sobol design number 30 [20]

Fin height	Fin length	Pitch	Strat angle
0.08 m	0.64 m	28.1°	33,3°

2.2 Numerical Simulation

Explanation including the governing equation which depicts the continuity equation carried out by Numerical simulation using RANSE and EASM; boundary condition describes the form of the boundary between the propeller and the environment, grid generation show that the shape of the grid in meshing meets convergence and grid independence condition.

2.2.1 Governing equations

The numerical simulation is carried out using continuity equation into unsteady conditions RANSE and EASM to solve the turbulence phenomena [21]. CFD simulation of PBCF succeed to obtained lower error margin compared to experiment results [22]. The equations are shown in Eq. (1), Eq. (2), and Eq. (3), respectively.

$$\frac{\partial \rho}{\partial t} + \frac{\partial (\rho u)}{\partial x} + \frac{\partial (\rho v)}{\partial y} + \frac{\partial (\rho w)}{\partial z} = 0 \tag{1}$$

Where u, v, and w are the vector field of flow speed, ρ is the density of the fluid, and t represents the time.

$$\frac{\partial U_i}{\partial t} + U_j \frac{\partial U_j}{\partial X_j} = \frac{\partial p}{\partial X_i} + \frac{\partial}{\partial X_j}\left[Re_{eff}^{-1}\left(\frac{\partial U_i}{\partial X_j} + \frac{\partial U_j}{\partial X_i}\right)\right] + \frac{1}{2}\left(\frac{\partial U_i}{\partial X_j} + \frac{\partial U_j}{\partial X_i}\right) \tag{2}$$

Where Reynolds average velocity components indicate by U_i = (u, v, w); the independent coordinate direction represent by x_i = (x, y, z); the mean strain-rate tensor for a body force denoted by S_i ; piezometric pressure symbolized by *p*, and effective Reynolds numbers denoted by Re_{eff}.

In Eq. (2), The Reynolds stress is modelled using EASM. The EASM's scientific establishment and specific derivation are refer to previous studies [4-7, 23] and shows the final result of the Algebraic Reynolds Stress Model for two-dimensional flow, which is briefly replicated here for comprehensiveness. The Reynolds stress tensor is obtained as follows:

$$\tau_{IJ} = 2\nu t\left(S_{ij} - \frac{1}{3}\frac{\delta_{uk}}{\delta_{xk}}\delta_{ij} + \left[a_2 a_4\left(S_{Ik}W_{kj} - W_{ik}S_{kj}\right) - 2_{a3a4}\left(S_{ik}S_{kj} - \frac{1}{3}S_{kl}S_{lk}\delta_{ij}\right)\right]\right) - \frac{2}{3}\rho k\delta_{ij} \tag{3}$$

The turbulent eddy viscosity is calculated from:

$$v_t = \frac{2}{3}k\delta_{IJ} + max(-k_{\alpha 1}, 0.0005\frac{k^2}{\epsilon}) \quad (4)$$

Where α is determined from the following equation:

$$(\alpha_1/\tau)^3 + p(\alpha_1/\tau)^2 + q(\alpha_1/\tau) + \mathrm{r} = 0 \quad (5)$$

Where τ = k/ϵ is turbulence time scale. While p obtained by:

$$p = -\frac{\gamma_1}{\eta^2\tau^2\gamma_0}, p = \frac{1}{(2\eta^2\tau^2\gamma_0)^2}(\gamma_1^2 - 2\eta^2\tau^2\gamma_0 a_1 - \frac{2}{3}\eta^2\tau^2\alpha_3^2 + 2R^2\eta^2\tau^2\alpha_2^2), \mathrm{r} = \frac{\gamma_1}{(2\eta^2\tau^2\gamma_0)^2} \quad (6)$$

Furthermore, it is applied to arrange the Reynold stress into a linear part and a residual part according to following equation:

$$\tau_{ij} = \left(\frac{2}{3}k\delta_{IJ} + 2vtS_{IJ}\right) + \tau_{ij}^r \quad \text{with} \quad \tau_{ij}^r = \tau_{ij}^{asm} - \frac{2}{3}k\delta_{IJ} + 2vtS_{IJ} \quad (7)$$

Where is τ_{ij}^{asm} obtained from algebraic stress equation (ASM), v_t is eddy viscosity, and k is kinematics.

2.2.2 Boundary conditions

This study explains that the boundary conditions of the b-series propeller are presented in Figure 2 and the particulars of the two domains can be seen in Table 3.

Table 3
Distance of model to the domain boundary

Location	Distances
(D) Propeller diameter	300 mm
(S1) Distances from propeller to inlet	3D
(S2) Distances from propeller to outlet	8D
(R) The distances from the propeller center to the wall	4D
(L) Propeller length from hub to boss cap fins	0.6D

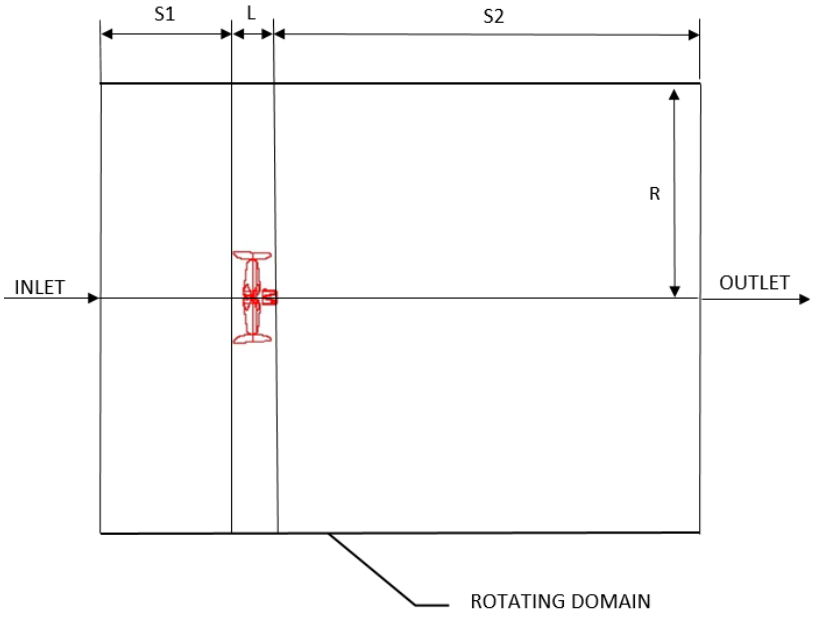

Fig. 2. Boundary conditions

The boundary conditions of the B-series propeller in this research are shown in Figure 2. Boundary condition in the Solid Model define as no-slipping. The inlet boundary condition is interpreted as the far field. Specified Pressure is used as the boundary condition at the outlet boundary. The Far Field boundary conditions are applied to the cylindrical surface so that the entire domain is the rotating domain. The rotating frame should be large enough to maintain the Far Field Boundary not affecting the simulation of the flow around the propeller. Furthermore, the intended domain is a cylinder with a 11D in length and 8D in diameter with the axis that coincides with the propeller's axis symmetry. The inlet is located 3D from the model and the outlet is located 8D from the model. Each size and distance of the two domains concluded in Table 3.

2.2.3 Grid generation

CFD Design was used to create the mesh, shown in Figure 3. Fine meshing was done to guarantee the sufficiency of the simulations [24]. Therefore, it is important to carry out grid independence study. The suitability of the mesh number also could be equalized to the working hours of computer calculations, which should be set to be effective and optimal [25]. Furthermore, the selection of mesh type and their arrangement influences the simulation results generated. The selection of the mesh order is proven to generate better results in CFD simulations. Simulation accuracy is able to be improved by applying finer grid around the model that interacts with the fluid, which lead to more proper interaction phenomena simulated. Meanwhile, distant part of the fluid can be arranged with larger grid size to reduce the simulation process. This setting provides more effective computer performance and accuracy results.

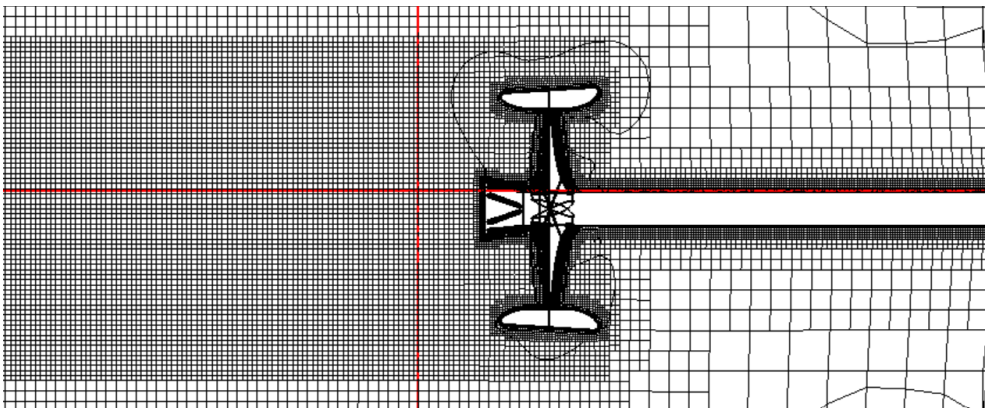

Fig. 3. Meshing of propeller model Ka4-70 with Nozzle 19A and PBCF divergent

Moreover, independence grids were added to several elements in the interest of getting constant number which can generate less error (Figure 4). Comparison of numerical and experimental indicate the error number is below 2% [26]. However, the value of <1% is preferred in the Table 4.

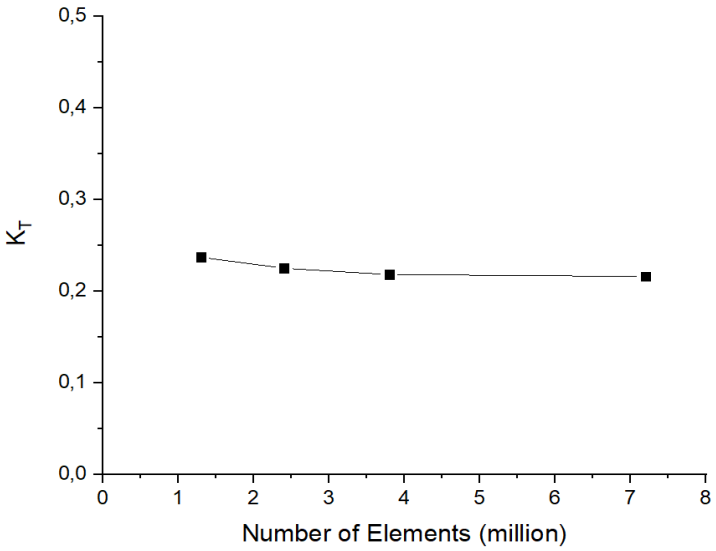

Fig. 4. Grid independence propeller Ka4-70 with Nozzle 19A and PBCF divergent for K_T

Table 4
Grid independence propeller Ka4-70 with Nozzle 19A and PBCF divergent

Number of element	1,258,299	2,344,576	3,835,380	7,190,246
K_T	0.237	0.225	0.218	0.216
Percentage	-	1.3%	0.7%	0.2%

2.3 Towing Test Model

When conducting propeller tests, it is important to consider and adjust the laboratory scale based on the capacity of the equipment [27]. It is necessary to obtain a test model that is constructed with sturdy materials and has precise dimensions. As a result, a balancing model is typically employed prior to testing to ensure equal weight distribution across each blade.

The experimental testing was conducted in a towing tank owned by LHI in Surabaya, Indonesia. The tank has the following dimensions: length of 234.5 meters, width of 11 meters, and depth of 5.5 meters. The maximum speed of the carriage used in the experiment was 8 m/s, with a maximum acceleration of 1 m/s². The length of the ship model used in the tests ranged from 3 to 9 meters. Figure 5 illustrates the physical setup of the towing tank.

Fig. 5. Towing tank at Indonesian Hydrodynamic Laboratory

The open water test system [28] is described as follows (see Figure 6 and Figure 7): (i) A dynamometer (H-39) equipped with strain gauge sensors is used for conducting the open water tests. These sensors convert the thrust and torque generated by the propeller into electrical signals measured in microstrain and then into mv/volt electricity. (ii) A Programmable Signal Conditioning (PSC) device is employed as a signal conditioner to determine the magnitude of thrust and torque produced by the dynamometer. The PSC includes a sensor voltage source, gain settings, and filter signals to convert the electrical measurements from the dynamometer. (iii) A Data Acquisition System (DAS) is responsible for collecting data from the sensors after they have been converted into electrical signals by the PSC. These signals are then converted into digital numbers using a calibration factor (voltage to torque thrust ratio) and stored in a computer for further processing and analysis.

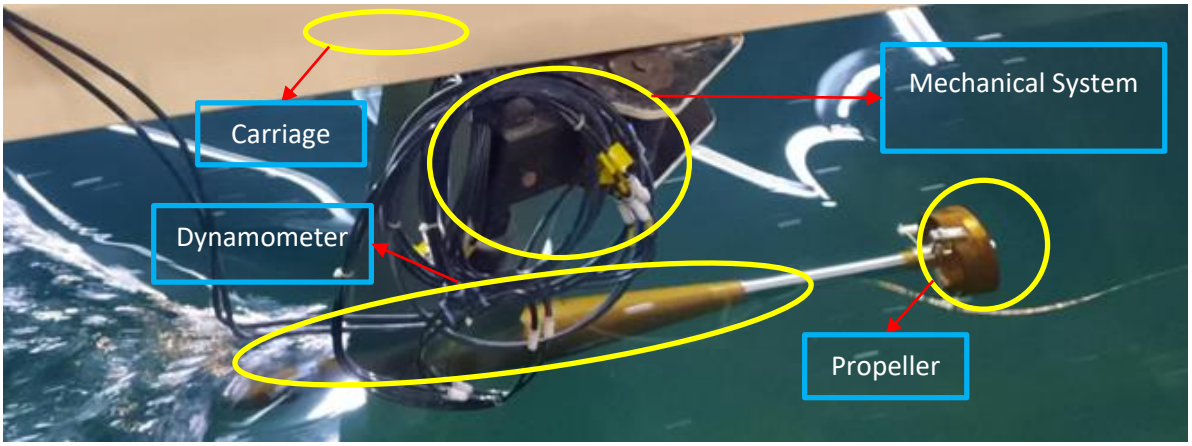

Fig. 6. Open Water Test

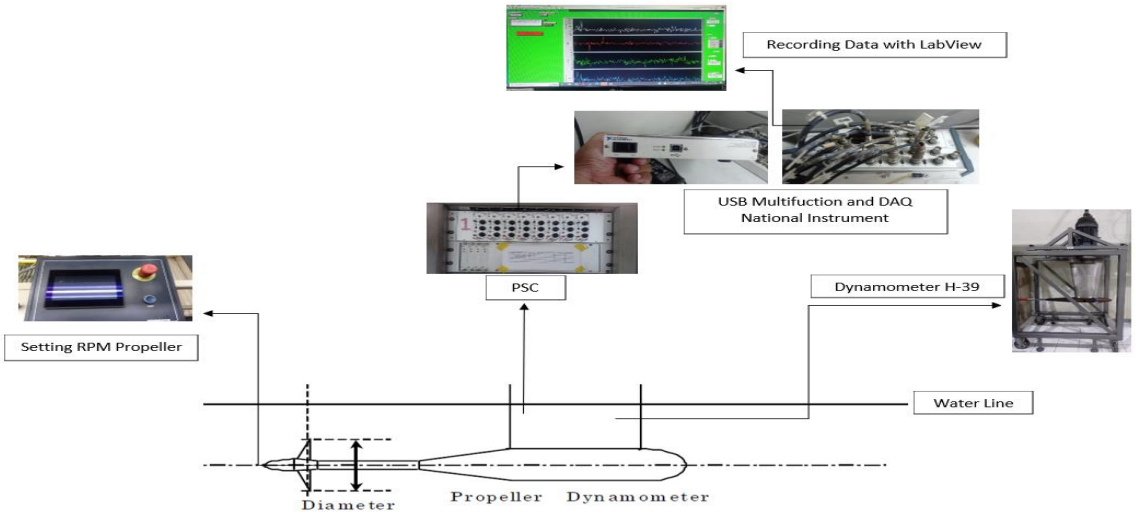

Fig. 7. Working system in towing tank for open water test

2.4 Propeller Efficiency

Propellers operate in the water are encountered by the ship as it sails. Therefore, propeller is mostly attached on ship's stern, which will impact its performance. Thus, it is required to operate the propeller in open water in order to examine the initial performance characteristics of a propeller, independent of the ship to which it is connected. A propeller's performance characteristics typically

refer to the deficit in its thrust, torque, and efficiency with advanced speed and rotation rate in open water.

Experiments are carried out with propeller model towed in the towing tank while vary the rotation rate and towing velocity to obtain the behavior of the propeller in open water. The propeller's thrust and torque are determined. The non-dimensional thrust K_T and torque K_Q (which is enhance 10 times as $10k_Q$ to be plotted in the same graph) are then presented as a function of advance coefficient J, along with open water efficiency η_0. Eq. (8) to (11) show the formulation of J, K_T, K_Q, η_0.

$$J = \frac{V_A}{nD} \tag{8}$$

$$K_T = \frac{T}{\rho n^2 D^4} \tag{9}$$

$$K_Q = \frac{Q}{\rho n^2 D^5} \tag{10}$$

$$\eta_0 = \frac{v_a}{2\pi nD}\frac{K_T}{K_Q} \tag{11}$$

3. Results and Discussion

Ka4-70 Propeller CFD calculations result with and without Nozzle 19A with PBCF Divergent are shown in Table 5 and Table 6, while the results of the Ka4-70 Propeller Experiment with Nozzle 19A and PBCF Divergent can be seen in Table 7. Moreover, the comparison of the results between the numerical and experiment test can be seen in Figure 8a, Figure 8b, and Figure 8c.

Table 5
CFD results for Ka4-70 propeller without Nozzle 19A and PBCF divergent

J	K_T	$10K_Q$	η_0
0.000	0.548	0.956	0.000
0.100	0.494	0.867	0.091
0.200	0.455	0.794	0.182
0.300	0,410	0.718	0.273
0.400	0.363	0.635	0.364
0.500	0.310	0.551	0.448
0.600	0.257	0.467	0.526
0.700	0.203	0.396	0.572
0.800	0.147	0.363	0.515
0.900	0.095	0.278	0.489
1.000	0.042	0.190	0.349

Table 6
CFD results for Ka4-70 propeller with Nozzle 19A and PBCF divergent

J	K_T	$10K_Q$	η_0
0.000	0.379	0.752	0.000
0.100	0.355	0.706	0.080
0.200	0.349	0.692	0.160
0.300	0.348	0.689	0.241
0.400	0.344	0.684	0.320
0.500	0.327	0.657	0.396
0.600	0.305	0.607	0.480
0.700	0.288	0.530	0.606
0.800	0.210	0.473	0.565
0.900	0.146	0.401	0.523
1.000	0.076	0.284	0.423

Table 7
Experimental results for Ka4-70 propeller with Nozzle 19A and PBCF divergent

J	K_T	$10K_Q$	η_0
0.0	0.349	0.613	0.000
0.1	0.330	0.588	0.089
0.2	0.298	0.555	0.171
0.3	0.240	0.484	0.236
0.4	0.223	0.450	0.316
0.5	0.210	0.407	0.412
0.6	0.189	0.365	0.495
0.7	0.158	0.319	0.551
0.8	0.126	0.284	0.566
0.9	0.087	0.240	0.520
1.0	0.044	0.191	0.366

Open Water Test for propeller model was done in Calm Water conditions based on ITTC regulations for open-water tests [29]. The results of the study succeed to present the value of K_T, $10K_Q$, and η_0 of Numerical simulation and experiments test. Comparison of Ka4-70 propeller without Nozzle 19A and PBCF divergent can be seen in Table 5 and Table 6 namely Ka4-70 propeller with Nozzle 19A and PBCF divergent, when without Nozzle and PBCF J = 0.1 K_T value is 0.494; J = 0.5 K_T value 0.310; J = 0.7 K_T value (0.203) compared to with Nozzle and PBCF when J = 0.1 K_T value is 0.379; J = 0.5 K_T value 0.327; J = 0.7 K_T value (0.288) shows that the K_T value of Open propeller ae higher when J = 0 to J = 0.4, and K_T are higher at J = 0.5 to 1.0. While Open propeller when J = 0.1 value $10K_Q$ 0.867; J = 0.5 value $10K_Q$ 0.551; J = 0.7 $10K_Q$ value (0.396) compared to Nozzle and PBCF when J = 0.1 $10K_Q$ value 0.706; J = 0.5 value $10K_Q$ 0.657; J = 0.7 value of $10K_Q$ (0.530) shows that $10K_Q$ value are higher at J = 0 to J = 0.3. however, $10K_Q$ value are lower at J =0.4 to J=1.0. Then the comparison is seen from Ka4-70 propeller without Nozzle 19A and PBCF divergent η_0 value when J = 0.1 value η_0 0.091; J = 0.5 value η_0 0.448; J = 0.7 value η_0 (0.572) compared to Nozzle and PBCF when J = 0.1 value η_0 0.080; J = 0.5 value η_0 0.396; J = 0.7 value η_0 0.606 shows that η_0 value of Open Propeller are higher on J=0 to J=0.6 but the value are lower at J =0.7 to J=1.0. Meanwhile, between CFD and the experiment can be seen from Table 6 and Table 7, the highest K_T value is in CFD, which is 0.379 when J = 0, then the highest $10K_Q$ value is in CFD, which is 0.752 when J (0), and the highest η_0 value is in CFD, which is 0.606 in J = 0.7.

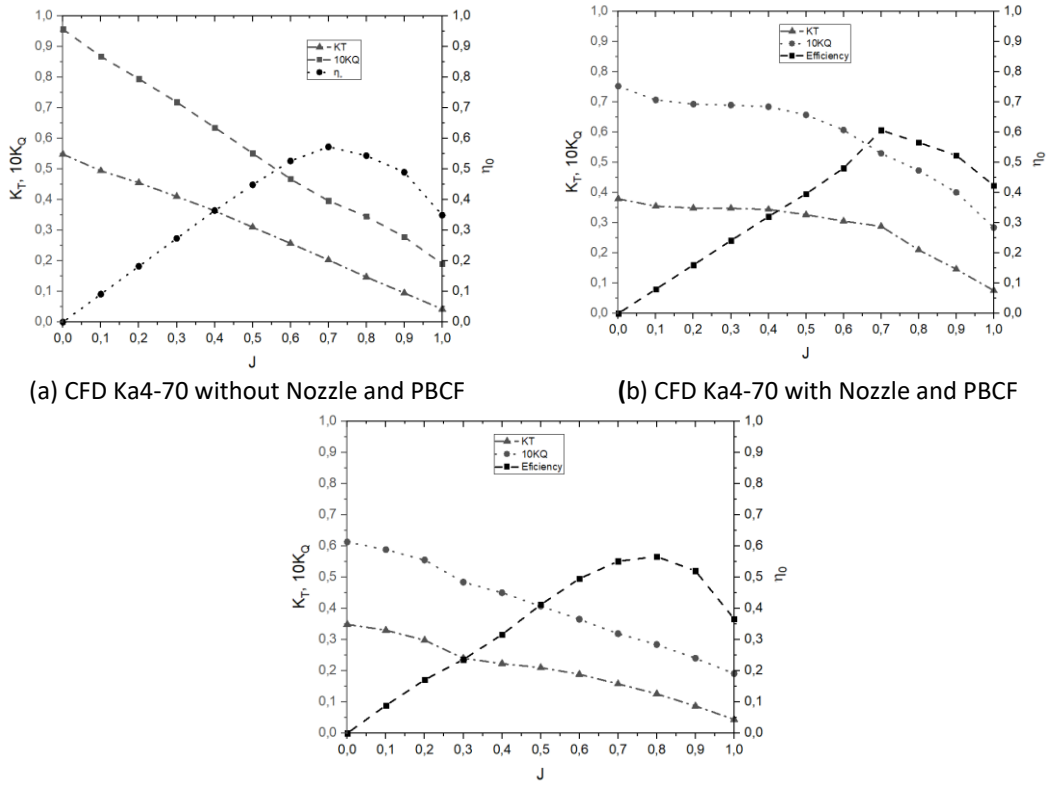

(a) CFD Ka4-70 without Nozzle and PBCF (b) CFD Ka4-70 with Nozzle and PBCF

(c) Experiment Ka4-70 with Nozzle and PBCF

Fig. 8. Open water test diagram CFD and experiment for Ka4-70 propeller with or without nozzle and PBCF

The process of plotting the open water test graph refers to the experimental graph by Wageningen series which the graph shows the results of the K_T, $10K_Q$, and Efficiency (η_0) values. Figure 8 conclude CFD simulation result of Ka4-70 propeller without Nozzle and PBCF, propeller Ka4-70 using Nozzle and PBCF, and experiment result of Ka4-70 propeller using Nozzle and PBCF. Simulation result of Ka4-70 propeller without nozzle and PBCF shows that the highest value of K_T and $10K_Q$ occur at J = 0 and lowest value of K_T and $10K_Q$ occur at J = 1.0. This result pattern also found on propeller Ka4-70 using Nozzle and PBCF either on CFD and Experimental results. Meanwhile, $\eta_0$value from CFD simulation of Ka4-70 propeller without Nozzle and PBCF shows the lowest value of η_0 occur at J = 0. Similiar trend value for η_0 also occur at Ka4-70 propeller using Nozzle and PBCF on CFD and experimental result. Highest η_0 value in CFD simulation occur at J = 0.7 and the highest one in experiment test occur at J = 0.8. Kaplan series propeller is better use a nozzle, its looks like the K_T value is bigger when J is high [30].

Visualization of Ka4-70 Propeller without Nozzle and PBCF Pressure support CFD simulation results in Table 5 and Figure 9. The results explain that at low speeds J = 0 highest K_T value is 0.548, and at moderate speeds J = 0.5 K_T value occur at 0.310; while at high speeds J = 0.7 the value of K_T is 0.203. In the boss cap, large pressure found when J = 0.1 ≥1000 Pa, J = 0.5 is ≥1000 Pa, and J = 0.7 is ≥1000 Pa. In this study, the Ka4-70 propeller without Nozzle and PBCF experienced large pressure at low-speed J = 0.1 to high-speed J = 0.7. Previous open propeller research shows large pressure[31].

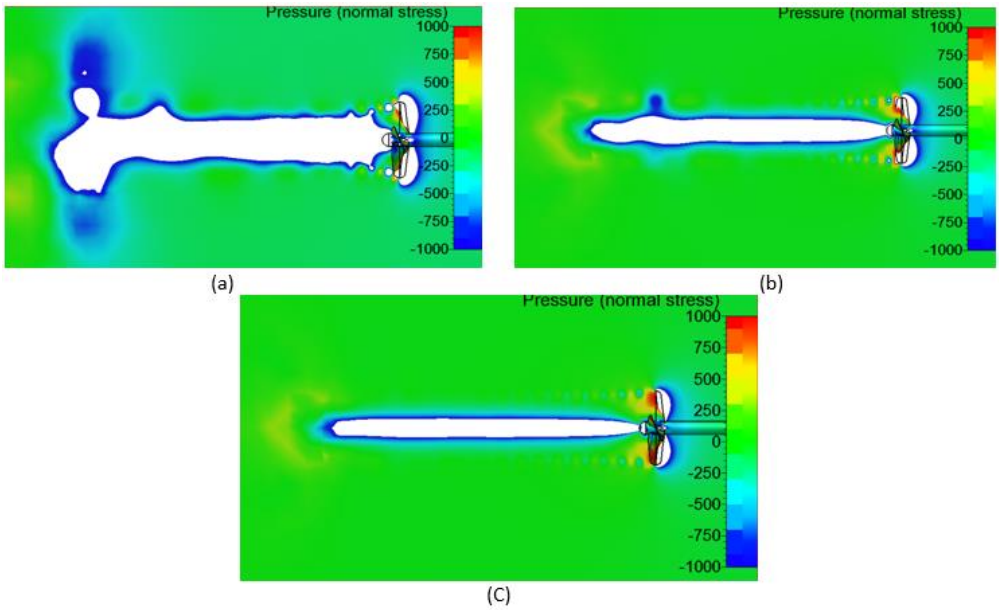

Fig. 9. Visualization of pressure Ka4-70 propeller without Nozzle 19 A and PBCF divergent (a) Pressure without nozzle and PBCF at J = 0.1 (b) Pressure without Nozzle and PBCF at J = 0.5 (c) Pressure without Nozzle and PBCF at J = 0.5

Visualization of Ka4-70 Propeller with Nozzle and PBCF Pressure corroborates CFD simulation results in Table 5 and Figure 10. The results concluded on the tables and graphs show that at J = 0.1 the K_T value is 0.355 and reduce when J = 0.5 K_T is 0.327 to lowest at J = 1.0 K_T 0.076. In the boss cap fins, large pressure occured when J = 0.1 ≥1000 Pa, while J = 0.5 ≥1000 Pa. However, the pressure value is small when J = 0.7 is ≥750 Pa. In this study, the Propeller Ka4-70 with Nozzle PBCF Divergent experienced a large pressure at low speeds J = 0.1 to J = 0.5, thus a solution was needed to decrease the pressure. While previous studies propeller ducted with different PBCF [32].

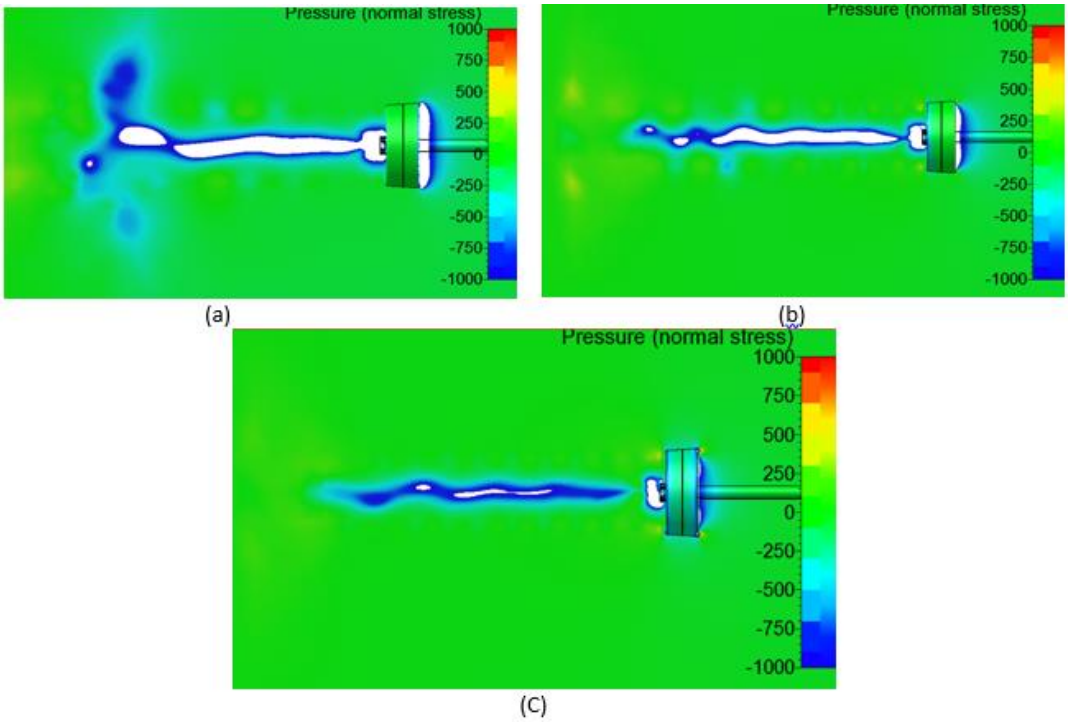

Fig. 10. Visualization of pressure propeller Ka4-70 with Nozzle 19A and PBCF divergent (a) Pressure with Nozzle PBCF at J= 0.1 (b) Pressure with Nozzle PBCF at J= 0.5 (C) Pressure with Nozzle PBCF at J= 0.7

The velocity of the Ka4-70 Propeller without Nozzle 19A and PBCF divergent strengthen the results of the CFD simulation for the pressure value (see Figure 11). In the boss cap fins, large pressure occur when J = 0.1 ≥1000 Pa, J = 0.5 is ≥1000 Pa, and J = 0.7 is ≥1000 Pa. In this study, the Ka4-70 propeller without Nozzle and PBCF encounter great pressure at low-speed J = 0.1 to high-speed J = 0.7, thus a solution was needed to decreas the pressure. The visualization of the velocity of the Ka4-70 Propeller without PBCF also support the CFD simulation results for the pressure value. Starting from J = 0.1 in the blade section, it induce axial velocity is 3 m/s to 4 m/s, but in the boss cap propeller, flow occurs at speeds of 0 m/s to 1 m/s. Whereas in the J = 0.5 blade section the induce axial velocity is 3 m/s to 4 m/s and in the propeller cap boss section the flow occurs at 0 m/s to 1 m/s. Meanwhile, when J = 0.7 is in the blade section the induce axial velocity is 3 m/s to 4 m/s, however, in the boss cap propeller section, flow occurs with speeds of 0 m/s to 2 m/s. In conclusion, the Ka4-70 propeller without 19A nozzle and PBCF Divergent increases the flow velocity at the boss cap fins but does not increase the axial induce velocity. Corroborates the case study of open propeller flow [33].

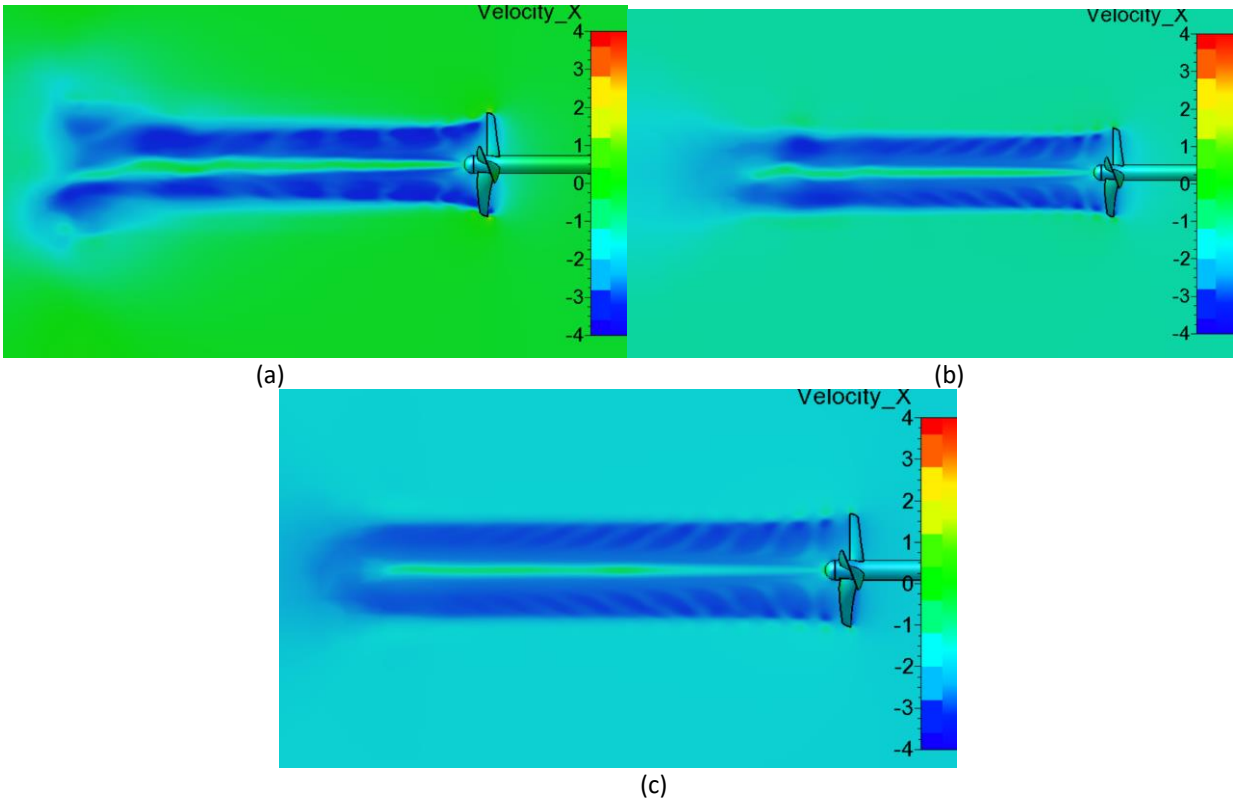

Fig. 11. Visualization of velocity Ka4-70 propeller without Nozzle 19A and PBCF divergent (a) Velocity without Nozzle PBCF at J = 0.1 (b) Velocity without Nozzle PBCF at J = 0.5 (c) Velocity without Nozzle PBCF at J = 0.7

The visualization for Ka4-70 Propeller velocity with nozzle and PBCF divergent support the CFD simulation results for the pressure on boss cap fins (see Figure 12). Large pressure take place when J = 0.1 ≥1000 Pa, while J = 0.5 ≥1000 Pa, while the smaller pressure occur when J = 0.7 is ≥750 Pa. In this study, the Propeller Ka4-70 with Nozzle 19A and PBCF divergent encounter large pressure at low speeds J = 0.1 to J = 0.5, thus, solution needed to reduce the pressure. The visualization of the velocity of the Propeller Ka4-70 with Nozzle 19A and PBCF divergent also corroborates the CFD simulation pressure results. Starts from J = 0.1 in the blade section, the induce axial velocity is 2 m/s to 3 m/s, but in the boss cap propeller, flow occurs with speeds of 0 m/s to 1 m/s. Whereas in the J = 0.5 blade section the induce axial velocity is 2 m/s to 4 m/s and in the propeller cap boss section the flow occurs

at 0 m/s to 1 m/s. Meanwhile, when J = 0.7 is in the blade section the induce axial velocity is 3 m/s to 4 m/s, however, in the boss cap propeller section, reverse flow occurs with a speed of 0 m/s to 1 m/s. In conclusion, Ka4-70 propeller using nozzle and PBCF divergent increases the axial induce velocity of the blade, but does not increase the flow velocity of the boss cap fins. Prove the fluid flow research that occurs in open propeller and ducted propeller [34].

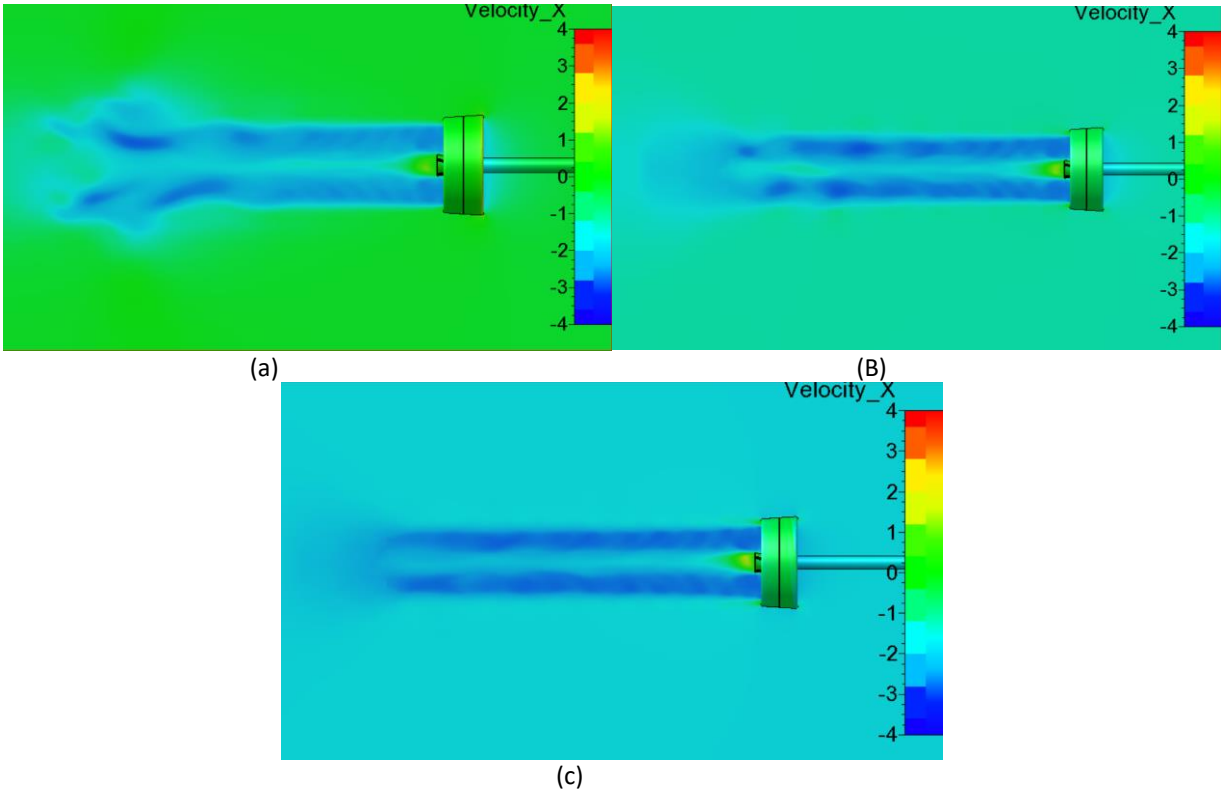

Fig. 12. Visualization of velocity propeller Ka4-70 with nozzle and PBCF divergent (a) Velocity nozzle PBCF at J= 0.1 (b) Velocity Nozzle PBCF at J= 0.5 (c) Velocity Nozzle PBCF Divergent at J= 0.7

The comparison result between Ka4-70 Propeller with and without Nozzle 19A and PBCF Divergent visualize in Figure 13, namely, K_T Nozzle and PBCF value increases from J = 0.6 to J = 1.0 when using Nozzle and PBCF. The value shows that it increase its value of K_T to 30%, and $10K_Q$ value at Ka4-70 with Nozzle 19A and PBCF divergent shows average increase value at J = 0.5 to J =1.0 in the amount of 25 %. K_T value are larger compared to $10K_Q$ using Nozzle 19A and PBCF divergent combination. η_0 value at J = 0.7 to J = 1.0 increased η_0 to 12%. Thus, Ka4-70 propeller without Nozzle and PBCF value increase of propeller η_0 [35] when added to ESD in the form of Nozzle and PBCF when J is high, from J = 0.7 to J = 1.0.

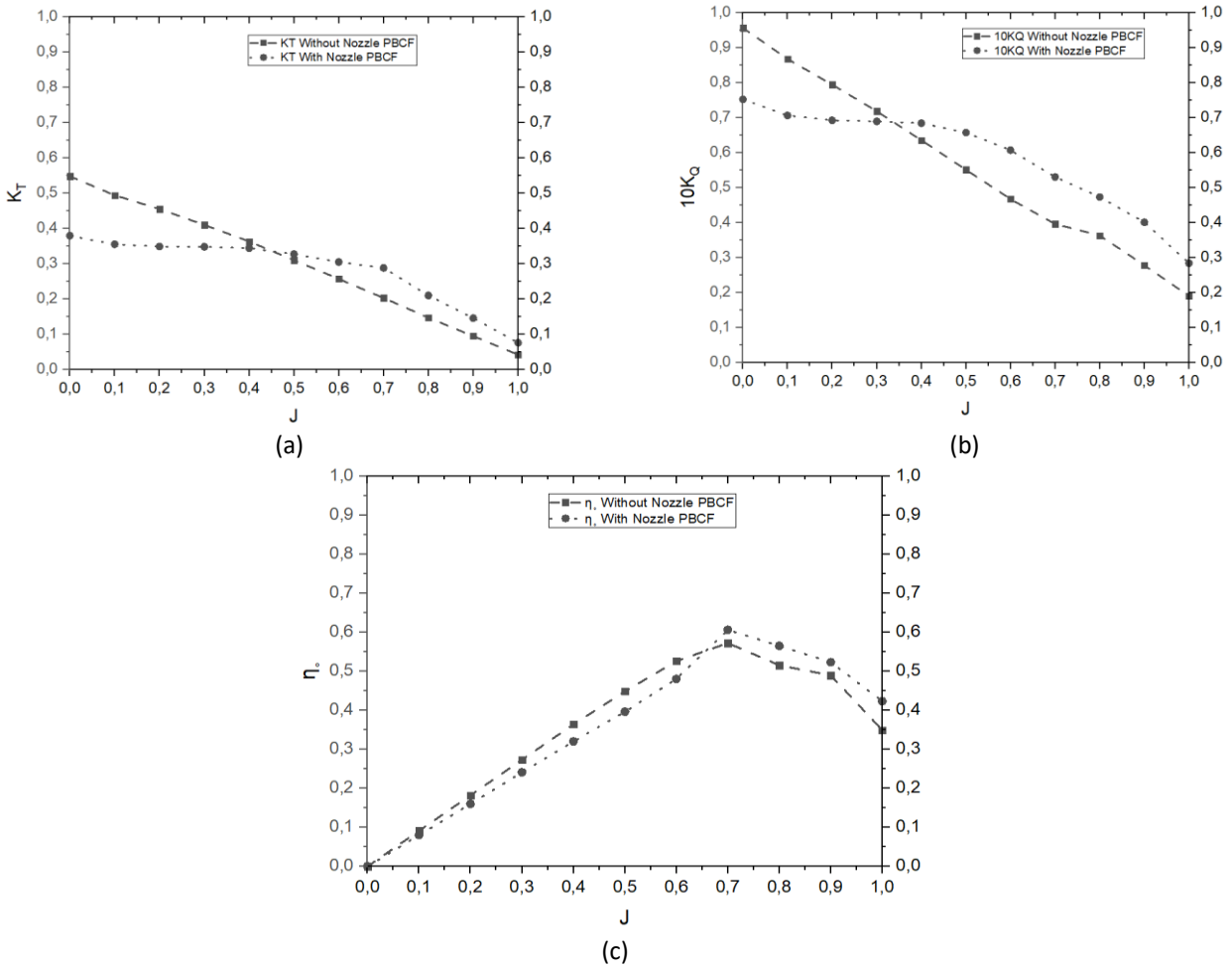

Fig. 13. Comparison open water test Ka4-70 propeller with and without Nozzle 19A and PBCF divergent (a) K_T value with and without Nozzle PBCF (b) $10K_Q$ value with and without Nozzle PBCF (c) Efficiency value CFD between with and without PBCF

The comparison result as shown in Figure 14 between numerical and experiments from Ka4-70 propellers with Nozzle 19A and PBCF Divergent show that some phenomena are occurred. In the $10K_Q$ graph, the first phenomenon shows the distance between J = 0 to J = 1.0 were strecthed, thus, further research is needed for torque. The second phenomenon for smaller values of J found in the K_T values on CFD and experiments, J=0 to J=0.2 shows narrow gap on the graph, while J= 0.3 to J =0.8 were stretched. Distance between CFD and experiment gap were smaller on J=0.9 to J=1.0. The last phenomenon of Ka4-70 propellers with Nozzle 19A and PBCF Divergent has very similar η_0 from J=0 to J=1.0, thus strengthen the study obtained about value results on CFD open and ducted propeller investigation [36]. Similar trend also occur on B4-70 Propeller research with additional boss cap fins where η_0 value at J = 0.8 to J = 1.0 increases by 3% to 8% [37]. Therefore, the overall simulation using the CFD approach are still valid to be relied upon as is the case in this paper.

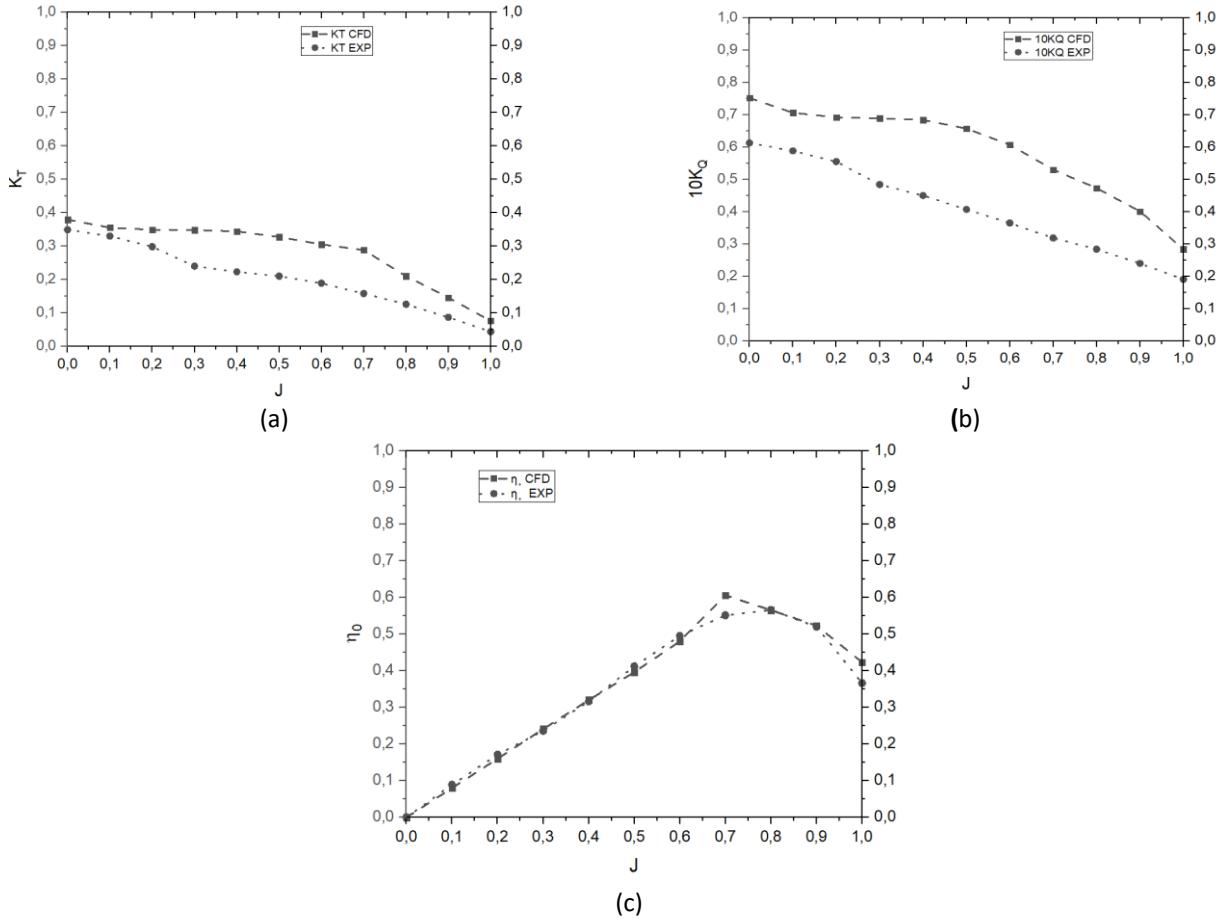

Fig. 14. Comparison open water test Ka4-70 propeller between CFD and experiment (a) K_T value between CFD and experiment (b) $10K_Q$ value between CFD and experiment (c) Efficiency value between CFD and experiment

4. Conclusions

The research was carried out using Reynolds Averaged Navier Stokes Equation (RANSE), which was validated by comparing the result value with experimental data from the open water test model. The Ka4-70 propeller design was designed to investigate ESD effect on propeller efficiency. Moreover, it was then utilized to assess the effect of PBCF. On a model scale, Numerical analysis was performed using CFD approach. The study's findings include a design that can be used for market ESD analysis.

The results of the comparative investigation cases between numerical and experiment analysis from Ka4-70 propellers with Nozzle 19A and PBCF Divergent appears that between CFD and experiments, several phenomena are seen. i) the Ka4-70 propeller without Nozzle 19A and PBCF divergent experienced large pressure at low-speed J = 0.1 to high-speed J = 0.7, but Ka4-70 propeller with Nozzle and PBCF divergent reach highest pressure at J = 0.1 to J = 0.5; ii) the Ka4-70 propeller without 19A nozzle and PBCF divergent increases the flow velocity at the boss cap fins but does not increase the axial induce velocity, while Ka4-70 propeller using nozzle and PBCF divergent increases the axial induce velocity of the blade, but does not increase the flow velocity of the boss cap fins; iii) Ka4-70 propeller without Nozzle and PBCF value increase of propeller η_0 to 12% when ESD added in the form of Nozzle and PBCF when J is high, from J = 0.7 to J = 1.0. ; iv) Ka4-70 propellers with Nozzle 19A and PBCF Divergent has very similar η_0 from J=0 to J=1.0. CFD approach are still appropriate to be relied upon for the overall simulation.

Acknowledgement
The authors wished to thank the Institut Teknologi Sepuluh Nopember for funding the research through a research scheme known as “Research for Doctoral Dissertation” under contract number: 1566/PKS/ITS/2022. The authors acknowledge the facilities, scientific and technical support form Hydrodynamics Laboratory, National Research and Innovation Agency. The first author would like to thank in particular to Diponegoro University for providing the funding the doctoral program. The authors would also like to Husein Syahab from Institut Teknologi Sepuluh Nopember, Surabaya, for his helps in working with CFD code.

References

[1] Bhattacharyya, Anirban, Vladimir Krasilnikov, and Sverre Steen. "A CFD-based scaling approach for ducted propellers." *Ocean engineering* 123 (2016): 116-130. https://doi.org/10.1016/j.oceaneng.2016.06.011.
[2] Luigi Stipa. 1932. Experiments with Intubed Propellers. Washington: L’Aerotecnica.
[3] Kort, L., 1934. Der Neue Dusenschrauben-antrieb. Werft, Reederei und Hafen.
[4] Van Manen, J.D., Oosterveld, M.W.C., 1966. Analysis of ducted propeller design. Trans. SNAME 74, 522–561.
[5] Mewis, Friedrich. "A novel power-saving device for full-form vessels." In *First International Symposium on Marine Propulsors, SMP*, vol. 9. 2009.
[6] Celik, Ishmail B., Urmila Ghia, Patrick J. Roache, and Christopher J. Freitas. "Procedure for estimation and reporting of uncertainty due to discretization in CFD applications." *Journal of fluids Engineering-Transactions of the ASME* 130, no. 7 (2008). https://doi.org/10.1115/1.2960953.
[7] MEPC, IMO. "1/Circ. 684 guidelines for voluntary use of the ship energy efficiency operational indicator (EEOI)." *International Maritime Organization: London, UK* (2009).
[8] Trimulyono, Andi, A. B. Jatmiko, I. P. Mulyatno, and H. Yudo. "The effect of propeller cap angle and fin size of PBCF on propeller performance." In *IOP Conference Series: Earth and Environmental Science*, vol. 972, no. 1, p. 012045. IOP Publishing, 2022. https://doi.org/10.1088/1755-1315/972/1/012045.
[9] Kiryanto, Mohammad Ridwan, Berlian Arswendo Adietya, Deddy Chrismianto, and Sri Hartanto Aji Sasongko. "Stability and total resistance analysis of catamaran fishing boat for Java North Sea area with hullform model and fishing gear variation." *International Journal of Mechanical Engineering and Technology (IJMET) Vol* 10, no. 01 (2019): 1291-1302.
[10] Ridwan, M., B. A. Adietya, and D. Chrismianto. "Stability analysis of trawls type traditional fishing boat with modification of eco-friendly fishing-gear on the north coast of Central Java." In *IOP Conference Series: Materials Science and Engineering*, vol. 403, no. 1, p. 012052. IOP Publishing, 2018. https://doi.org/10.1088/1757-899X/403/1/012052.
[11] Chrismianto, Deddy, Ahmad Fauzan Zakki, Berlian Arswendo, and Insanu Abdilla Cendikia Abar. "Comparison of Propeller Type B-Series and Au-Outline Gawn Series for Improving on Submarine Propulsion Performance using CFD." *International Journal of Advanced Research in Engineering and Technology* 10, no. 2 (2019).
[12] Adietya, Berlian Arswendo, Aulia Windyandari, and Ahmad Fauzan Zakki. "The Study on Stability and Seakeeping Characteristics of the Glass Bottom Boat Trimaran in Karimunjawa Island." In *IOP Conference Series: Earth and Environmental Science*, vol. 135, no. 1, p. 012007. IOP Publishing, 2018. https://doi.org/10.1088/1755-1315/135/1/012007.
[13] Ariana, I. Made, Riyan Bagus Prihandanu, Dhimas Widhi Handani, and A. A. B. Dinariyana. "Investigation of the Effects of the Pre-Duct in a Ship on Propeller–Hull Interactions Using the CFD Method." *CFD Letters* 15, no. 4 (2023): 17-30. https://doi.org/10.37934/cfdl.15.4.1730.
[14] Munggau, Dominic Laja, Djamal Hissein Didane, Sami Al-Alimi, Yazid Abdullsameea Mohammed Saif, and Bukhari Manshoor. "Computational Study on the Influence of Duct on The Performance of Darrieus Hydro-Turbine." *Journal of Advanced Research in Fluid Mechanics and Thermal Sciences* 105, no. 1 (2023): 210-219. https://doi.org/10.37934/arfmts.105.1.210219.
[15] Bahambary, Khashayar Rahnamay, and Brian Fleck. "A study of inflow parameters on the performance of a wind turbine in an atmospheric boundary layer." *Journal of Advanced Research in Numerical Heat Transfer* 11, no. 1 (2022): 5-11.
[16] Alias, Mohammad Azrul Rizal, Mohd Al Hafiz Mohd Nawi, Mohd Sharizan Md Sarip, Md Tasyrif Abdul Rahman, Muhamad Silmie Mohamad Shabri, and Raja Muhammad Zulkifli Raja Ibrahim. "Twist Blade Distributor in Fluidization Systems: Part 1–The Computational Procedure." *Journal of Advanced Research in Applied Sciences and Engineering Technology* 29, no. 2 (2023): 1-11. https://doi.org/10.37934/araset.29.2.111.

[17] Wallin, Stefan. 2000. *"Engineering Turbulence Modelling for CFD with a Focus on Explicit Algebraic Reynolds Stress Models."* Stockholm.
[18] Xing, L. H., G. B. Huang, and Min Yan. "Numerical Simulation of 3D Density Flow by an Improved EASM Model." *Procedia Environmental Sciences* 10 (2011): 753-758. https://doi.org/10.1016/j.proenv.2011.09.122.
[19] Bahatmaka, Aldias, Aditya Rio Prabowo, and Dong-Joon Kim. "Effect of Nozzle Performance on the Ducted Propeller: A Benchmark-Simulation Study using OpenFOAM." *Transportation Research Procedia* 55 (2021): 645-652. https://doi.org/10.1016/j.trpro.2021.07.031.
[20] Mizzi, Kurt, Yigit Kemal Demirel, Charlotte Banks, Osman Turan, Panagiotis Kaklis, and Mehmet Atlar. "Design optimisation of Propeller Boss Cap Fins for enhanced propeller performance." *Applied Ocean Research* 62 (2017): 210-222. https://doi.org/10.1016/j.apor.2016.12.006.
[21] Versteeg, Henk Kaarle, and Weeratunge Malalasekera. *An introduction to computational fluid dynamics: the finite volume method*. Pearson education, 2007.
[22] Kawamura, Takafumi, Kazuyuki Ouchi, and Takeo Nojiri. "Model and full scale CFD analysis of propeller boss cap fins (PBCF)." *Journal of marine science and technology* 17 (2012): 469-480. https://doi.org/10.1007/s00773-012-0181-2.
[23] Numeca International - Cadence Design Systems. n.d. *"FINEMarine-Theory-Guide."*
[24] Ismail, Iman Fitri, Akmal Nizam Mohammed, Bambang Basuno, Siti Aisyah Alimuddin, and Mustafa Alas. "Evaluation of CFD Computing Performance on Multi-Core Processors for Flow Simulations." *Journal of Advanced Research in Applied Sciences and Engineering Technology* 28, no. 1 (2022): 67-80. https://doi.org/10.37934/araset.28.1.6780.
[25] Abobaker, Mostafa, Sogair Addeep, Lukmon O. Afolabi, and Abdulhafid M. Elfaghi. "Effect of Mesh Type on Numerical Computation of Aerodynamic Coefficients of NACA 0012 Airfoil." *Journal of Advanced Research in Fluid Mechanics and Thermal Sciences* 87, no. 3 (2021): 31-39. https://doi.org/10.37934/arfmts.87.3.3139.
[26] Andersson, Bengt, Ronnie Andersson, Love Håkansson, Mikael Mortensen, Rahman Sudiyo, and Berend Van Wachem. *Computational fluid dynamics for engineers*. Cambridge university press, 2011.
[27] Ramli, Muhammad Ridzwan, Wan Mazlina Wan Mohamed, Hamid Yusoff, Mohd Azmi Ismail, Ahmed Awaludeen Mansor, Azmi Hussin, and Aliff Farhan Mohd Yamin. "The Aerodynamic Characteristics Investigation on NACA 0012 Airfoil with Owl's Wing Serrations for Future Air Vehicle." *Journal of Advanced Research in Fluid Mechanics and Thermal Sciences* 102, no. 1 (2023): 171-183. https://doi.org/10.37934/arfmts.102.1.171183.
[28] Data Acquisition Process from National Instrument.
[29] Procedures, Recommended. "Guidelines, Testing and Extrapolation Methods Propulsion, Propulsor, Open water test." In *Proceedings of the 25th International Towing Tank Conference (ITTC), Venice, Italy*, pp. 8-14. 2002.
[30] Gaggero, Stefano, Diego Villa, Giorgio Tani, Michele Viviani, and Daniele Bertetta. "Design of ducted propeller nozzles through a RANSE-based optimization approach." *Ocean Engineering* 145 (2017): 444-463. https://doi.org/10.1016/j.oceaneng.2017.09.037
[31] Eom, Myeong-Jin, Yoon-Ho Jang, and Kwang-Jun Paik. "A study on the propeller open water performance due to immersion depth and regular wave." *Ocean Engineering* 219 (2021): 108265. https://doi.org/10.1016/j.oceaneng.2020.108265
[32] Gaggero, Stefano, and Mattia Martinelli. "Comparison of different propeller boss cap fins design for improved propeller performances." *Applied Ocean Research* 116 (2021): 102867. https://doi.org/10.1016/j.apor.2021.102867
[33] Andersson, Jennie, Arash Eslamdoost, Marko Vikström, and Rickard E. Bensow. "Energy balance analysis of model-scale vessel with open and ducted propeller configuration." *Ocean Engineering* 167 (2018): 369-379. https://doi.org/10.1016/j.oceaneng.2018.08.047
[34] Gong, Jie, Chun-yu Guo, Da-gang Zhao, Tie-cheng Wu, and Ke-wei Song. "A comparative DES study of wake vortex evolution for ducted and non-ducted propellers." *Ocean engineering* 160 (2018): 78-93. https://doi.org/10.1016/j.oceaneng.2018.04.054
[35] Villa, Diego, Stefano Gaggero, Giorgio Tani, and Michele Viviani. "Numerical and experimental comparison of ducted and non-ducted propellers." *Journal of Marine Science and Engineering* 8, no. 4 (2020): 257. https://doi.org/10.3390/jmse8040257
[36] Adietya, Berlian Arswendo, I Ketut Aria Pria Utama, Wasis Dwi Aryawan, and Sutiyo. "CFD Analysis into the Effect of Using Propeller Boss Cap Fins (PBCF) on Open and Ducted Propellers, Case Study with Propeller B-Series and Kaplan-Series." *CFD Letters* 14, no. 4 (2022): 32–42. https://doi.org/10.37934/cfdl.14.4.3242
[37] Adietya, Berlian Arswendo, I. Ketut Aria Pria Utama, Wasis Dwi Aryawan, Mochammad Nasir, Mahendra Indiaryanto, Nurwidhi Asrowibowo, and Rizqi Dian Permana. "Numerical and Experimental Investigations into the Characteristics of Wageningen B4-70 Series of Propeller with Boss Cap Fins." *CFD Letters* 15, no. 10 (2023): 152-169. https://doi.org/10.37934/cfdl.15.10.152169